TOPOLOGICAL SYSTEMS

Generation of helical topological exciton-polaritons

Wenjing Liu[1], Zhurun Ji[1], Yuhui Wang[1], Gaurav Modi[1], Minsoo Hwang[1], Biyuan Zheng[2], Volker J. Sorger[3], Anlian Pan[2], Ritesh Agarwal[1]*

Topological photonics in strongly coupled light-matter systems offer the possibility for fabricating tunable optical devices that are robust against disorder and defects. Topological polaritons, i.e., hybrid exciton-photon quasiparticles, have been proposed to demonstrate scatter-free chiral propagation, but their experimental realization to date has been at deep cryogenic temperatures and under strong magnetic fields. We demonstrate helical topological polaritons up to 200 kelvin without external magnetic field in monolayer WS_2 excitons coupled to a nontrivial photonic crystal protected by pseudo time-reversal symmetry. The helical nature of the topological polaritons, where polaritons with opposite helicities are transported to opposite directions, is verified. Topological helical polaritons provide a platform for developing robust and tunable polaritonic spintronic devices for classical and quantum information-processing applications.

The recognition of the role of topology in condensed matter systems provided a route for understanding and creating new phases of quantum matter and exploring new phenomena and their applications (*1*). Topologically inequivalent insulators cannot be adiabatically transformed into one another without a phase transition that involves closing the bandgap. As such, the transport through interface states formed at the boundary of topologically inequivalent insulators is topologically protected and free from back-scattering by various defects. Depending on the presence of time-reversal symmetry, two-dimensional (2D) topological insulators can be broadly divided into two classes: quantum Hall (QH) systems, which support chiral charge currents, and quantum spin Hall (QSH) systems, which support helical spin currents. With the extension of the topological formalism to photonic systems (*2*), topological photonics is now an active research field (*3*). Photonic analogs of QH and QSH effects have been demonstrated (*4*–*7*), which gave rise to topological devices including robust waveguides, routers, and lasers (*8*–*10*).

Polaritons have emerged as an important platform for exploring new topological matter that bridges electronic and photonic systems (*11*–*19*). Exciton-polaritons are half-light, half-matter quasiparticles resulting from the strong hybridization between excitons and photons when the coherent energy transfer rate between them exceeds their decay rates. Proposals on realizing topological polaritonic states use excitons in a topologically nontrivial system (*17*), the spin-orbit coupling of photons (*16*), or the photon-exciton hybridization process (*11*), allowing manipulation of topological properties by independent control of each component (*20*). Compared with bare photonic systems, the excitonic component in polaritons introduces strong interparticle interactions and enhanced sensitivity to external stimuli that can be useful for assembling nonlinear and actively controllable topological devices.

Recently, a 2D polaritonic QH system was experimentally achieved in quantum-well lattices with nontrivial topology originating from the TE-TM splitting of the photonic mode and the topological bandgap opened by the Zeeman splitting of excitons. Although this is a promising demonstration of a new phase of topological matter, the small bandgap (~0.1 meV) opened under strong magnetic fields and the 4 K operation temperature may restrict its widespread utilization. Fortunately, it is possible to avoid these challenges in an analogous QSH polaritonic system. QSH insulators do not require a magnetic field or magnetic order, and their optical analogs can be realized solely by exploiting the system symmetry and interactions with large topological bandgaps (>10 meV), thus providing opportunities for high-temperature operation. In addition, the additional spin-degree of freedom and helical nature of the analog QSH polaritons can be further exploited for polariton-based spintronic devices.

Here, we demonstrate helical topological polaritons in an analogous QSH system by strongly coupling monolayer WS_2 excitons with a topologically nontrivial hexagonal photonic crystal (Fig. 1). The polariton topology is protected by a pseudo time-reversal symmetry originating from the C_{6v} symmetry of the coupled system. Analogous to the helical edge states in a QSH insulator, topological exciton-polaritons in this system are distinct from their trivial counterparts. Polaritons of different helicity propagate in opposite directions and are topologically protected from back-scattering. Monolayer transition metal dichalcogenides are excellent candidates for exploring 2D polaritonic physics at higher temperatures because of their large exciton oscillator strength (*21*–*25*), and their ultrathin geometry ensures minimum perturbation to the band structure of the underlying photonic crystal.

Our photonic crystals are formed of hexagonal lattices, with each unit cell composed of six particles located on the perpendicular bisector of its six sides (Fig. 2A) (*6*, *7*, *26*–*28*). While keeping the sixfold rotational symmetry intact, the six particles can be simultaneously arranged toward or away from the unit cell center, which changes the intercell and intracell nearest-neighbor couplings. The topology of the lattice is controlled by swapping the intercell and intracell coupling strengths

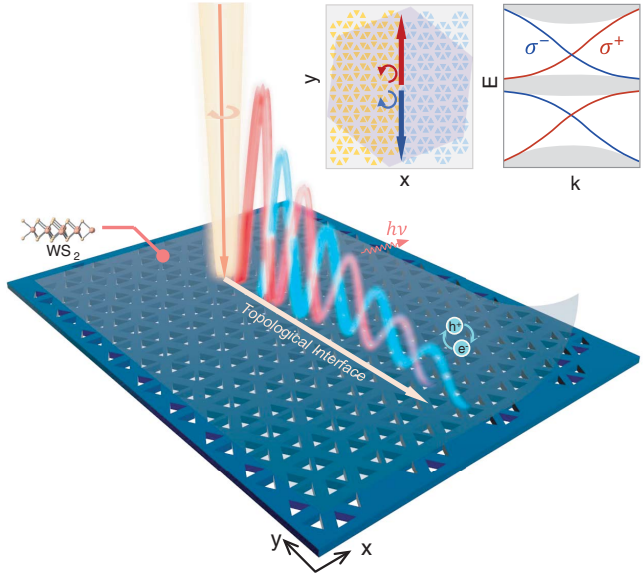

Fig. 1. Schematic of the helical topological polariton system. The topological polaritonic system consists of monolayer WS_2 strongly coupled to a nontrivial photonic crystal. Spin momentum–locked helical topological polaritons are confined to the domain wall connecting the two bulk lattice regions with different topology. Inset is a top view of the topological polariton device and a schematic of the helical polariton dispersion.

[1]Department of Materials Science and Engineering, University of Pennsylvania, Philadelphia, PA 19104, USA. [2]Key Laboratory for Micro-Nano Physics and Technology of Hunan Province, State Key Laboratory of Chemo/Biosensing and Chemometrics, College of Materials Science and Engineering, Hunan University, Changsha, Hunan 410082, P. R. China. [3]Department of Electrical and Computer Engineering, George Washington University, Washington, DC 20052, USA.
*Corresponding author. Email: riteshag@seas.upenn.edu

(*29*). We need to consider the coupling between such a photonic crystal and the A-excitons with isotropic polarization in monolayer WS_2 (*24*). The excitonic material was divided into six sublattices corresponding to each photonic unit cell. The tight-binding approximation was then applied by treating each of these sublattices as an isolated excitonic particle located at its mass center (Fig. 2A). The coupled system thus contains two particles within each sublattice corresponding to the excitonic and photonic structures, respectively. The Hamiltonian of the coupled system can be written as (see the supplementary materials, section 1A) follows:

$$H = \hbar \sum_i (\omega_{ph} \hat{a}_i^\dagger \hat{a}_i + \omega_{ex} \hat{b}_i^\dagger \hat{b}_i) + \sum_{NN} (f_{ij} \hat{a}_i^\dagger \hat{a}_j + H.c.) + g \sum_i (\hat{a}_i^\dagger \hat{b}_i + H.c.) \quad (1)$$

where $\hat{a}$ ($\hat{a}^\dagger$) and $\hat{b}$ ($\hat{b}^\dagger$) are the annihilation (creation) operators for photons and excitons, respectively; i,j = 1,2,...,6 are the six sublattices; $\hbar\omega_{ph}$ and $\hbar\omega_{ex}$ are the energies of the uncoupled photons and excitons, respectively; g_{ij} is the exciton-photon coupling strength; f_{ij} is the nearest-neighbor coupling factor of the photonic lattice, which is t_1 for the intracell coupling and $t_2 \exp(i\boldsymbol{k}\cdot\boldsymbol{a_i})$ for the intercell coupling, with $\boldsymbol{a_i}$ being the lattice vector.

Based on the C_{6v} symmetry of the exciton-photon coupled system, the Hamiltonian can be projected onto the basis $(|p_\pm^{ph}\rangle, |d_\pm^{ph}\rangle, |p_\pm^{ex}\rangle, |d_\pm^{ex}\rangle)^T$, where p and d denote modes with odd and even parities, respectively, and + or – signs represent pseudospin-up or pseudospin-down states associated with the positive or negative angular momenta, respectively. Near the Γ point of the Brillouin zone, the pseudospin-up and pseudospin-down states are decoupled and degenerate, each leading to four polariton bands (see the supplementary materials, section 1A):

$$\lambda_{upper} = \hbar\omega_0 + \frac{1}{2}\left(\pm\alpha + \sqrt{4g^2 + (\mp\alpha + \delta_{ep})^2}\right)$$
$$\lambda_{lower} = \hbar\omega_0 + \frac{1}{2}\left(\pm\alpha - \sqrt{4g^2 + (\mp\alpha + \delta_{ep})^2}\right) \quad (2)$$

where upper and lower denote the bands above and below the exciton energy ω_{ex}, respectively, $\omega_0 = \frac{1}{2}(\omega_{ex} + \omega_{ph})$, $\delta_{ep} = \hbar(\omega_{ex} - \omega_{ph})$, and α corresponds to the dispersion of the uncoupled photonic crystal with $\alpha = (t_2 - t_1)^2 + \frac{3}{4}t_2^2 k^2$. When $t_1 = t_2$, the two upper and lower polariton bands are degenerate at the Γ point with linear dispersion for small k values. These represent two Dirac cones with energy splitting of $\sqrt{4g^2 + \delta_{ep}^2}$, and a typical polariton dispersion can be characterized by a bulk band Rabi splitting, $\Omega_{bulk} = 2g$. This degenerate condition is the topological phase transition point of the designed exciton-photon coupled system. If $t_1 \neq t_2$, then a finite "mass" term is induced by α, which opens a bandgap in both the upper and lower Dirac cones (Fig. 2, B and C), with two different topological phases identified for $t_1 > t_2$ and $t_1 < t_2$ conditions, respectively (see the supplementary materials, section 1A). The topological phase transition can also be clearly observed by the inversion of band parity near the Γ point (Fig. 2, B and C) at both the upper and lower bandgaps: For $t_1 > t_2$, the band below each bandgap has an odd parity ($|p\rangle$ band), whereas the band above the bandgap has an even parity ($|d\rangle$ band), which reverses for the $t_1 < t_2$ condition.

Finite-difference time-domain (FDTD) simulations were performed on a WS_2-photonic crystal coupled structure (Figs. 1 and 2) that confirmed the predictions of the tight-binding model (see the supplementary materials, sections 2A to 2C). The key for obtaining a topologically nontrivial phase in the coupled system is the preservation of the C_{6v} symmetry, which is fulfilled by isotropic WS_2 excitons (*24*). The helical topological polariton interface states were extracted analytically by solving the real space wavefunction of the interface polaritons. For a polaritonic system with $t_2 > t_1$ at $x < 0$, and $t_2 < t_1$ at $x > 0$, the topological interface mode can be written as follows [see the supplementary materials, section 1B (*7*)]:

$$|\Psi\rangle = \begin{cases} \Sigma_i A_i |\phi_i^A\rangle \exp(ik_{y,i}^A y) \exp(|\delta_x^A| x) & for\ x < 0 \\ \Sigma_i B_i |\phi_i^B\rangle \exp(ik_{y,i}^B y) \exp(-|\delta_x^B| x) & for\ x > 0 \end{cases} \quad (3)$$

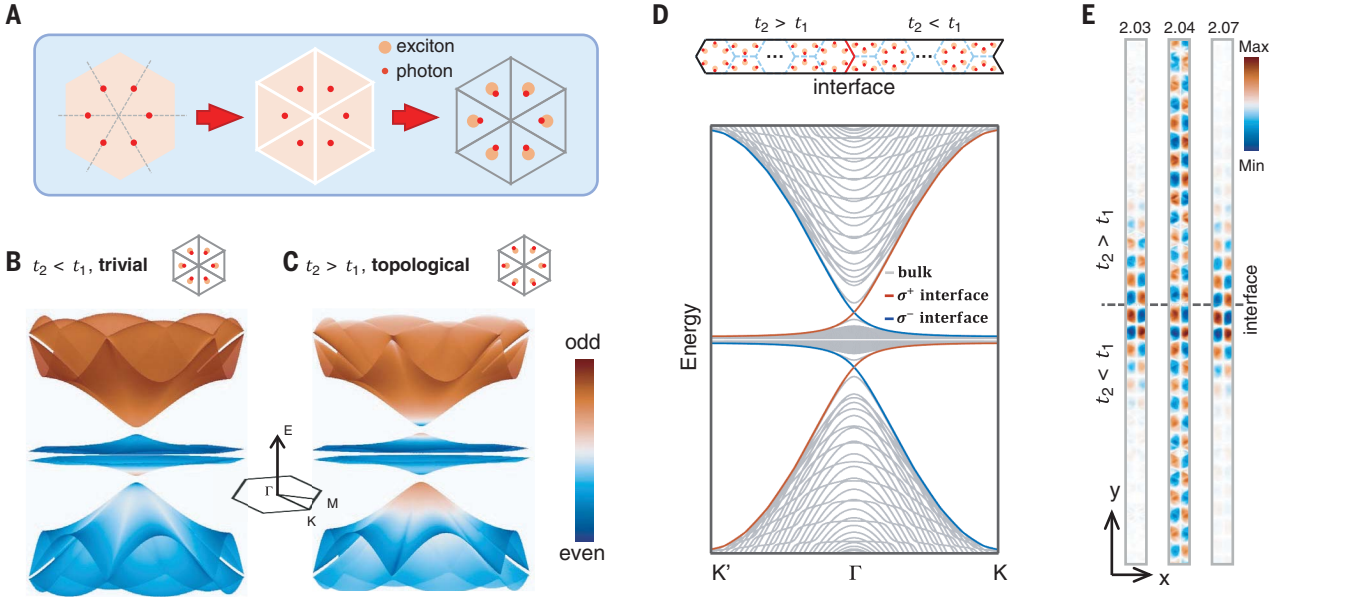

Fig. 2. Theoretical and numerical studies of the helical topological exciton-polaritons. (**A**) Illustration of the tight-binding model. The coupled structure contains six photonic resonators (red dots) in each hexagonal unit cell. The 2D excitonic layer (orange) is divided into six sublattices according to the photonic lattice symmetry, and excitonic particles are assumed to be located at the mass center of each sublattice. (**B** and **C**) Calculated band structures of the trivial and topological polaritonic lattices. The color plots the spatial parity of the bands. (**D**) Helical topological interface polariton states calculated from two polaritonic crystals with different topology connected by a zigzag domain wall. The pseudospin-up (red) and pseudospin-down (blue) interface polariton bands are associated with the positive and negative group velocities, respectively. (**E**) Spatial H_z field distribution of the WS_2-photonic crystal system at the domain wall calculated at 2.03 and 2.07 eV (two polaritonic Dirac points with field confinement) and at 2.04 eV, where the field extends into the bulk region between the Dirac points (fig. S2E).

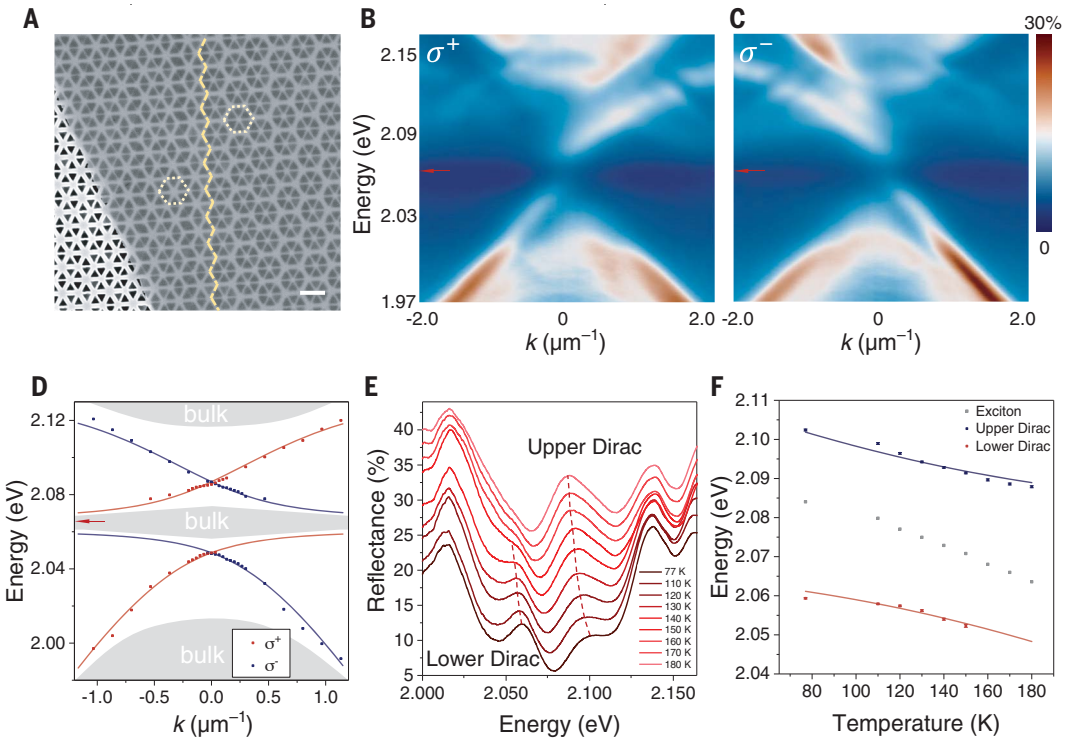

Fig. 3. Identification of the helical topological polaritons through momentum-space reflectance spectra. (**A**) Scanning electron microscope image of the WS_2-photonic crystal coupled structure at the topological domain wall (yellow dashed line). Scale bar, 500 nm. (**B** and **C**) Angle-resolved reflectance spectra of the helical interface polaritons excited by σ^+ and σ^- polarized light. The red arrows indicate exciton energy. (**D**) Topological polariton dispersion extracted from (B) and (C), fitted by the tight-binding model. (**E**) Reflectance spectra taken at the interface with k = 0 at varying temperature. (**F**) Temperature evolution of the upper and lower polaritonic Dirac points extracted from (E) and fitted to the tight-binding model. The error bars in (D) and (F) (<4 × 10^{-4} eV) are small compared with the energy range of the plot (see the supplementary materials, section 3B).

which is propagating along the y direction while evanescently decaying in the x direction. Here, $|\phi_i^A\rangle$ and $|\phi_i^B\rangle$ are the eigenfunctions for $x < 0$ and $x > 0$ and k_y and $|\delta_x|$ are the wave vector and decay constant along and perpendicular to the interface, respectively. The interface polariton dispersion can subsequently be obtained as follows (for pseudospin-up states):

$$E_{\pm} = \hbar\omega_0 + \frac{1}{2}\hbar v k_y \pm \frac{1}{2}\sqrt{4g^2 + (-\hbar v k_y + \delta_{ep})^2} \quad (4)$$

where $v = \frac{\sqrt{3}}{2}a_0 t_2$, and the + and – signs represent the upper and lower branches of the topological interface polariton modes, respectively. The dispersion curves always have a positive group velocity, whereas a set of interface polariton dispersions with opposite group velocities can be found for pseudospin-down states, therefore demonstrating the helical nature of the topological interface polaritons. The dispersion described by Eq. 4 exhibits an anticrossing behavior at the exciton energy that is characteristic of exciton-polariton dispersion, in which the Rabi frequency, Ω_{topo} = $2g$, is the same as the Rabi frequency of the bulk polariton, i.e., Ω_{bulk}. Although this result was obtained from a simplified tight-binding model, such consistency demonstrates that the anticrossing in the topological interface polariton bands is a direct consequence of the eigenmode splitting in the bulk polariton lattice, which can be viewed as the expression of the bulk-edge correspondence principle in the strong coupling regime. In other words, there are two equivalent descriptions of the anticrossing feature in the topological interface polaritonic dispersion: strong coupling between the exciton and the photonic interface state and, equivalently, the consequence of nontrivial topology of the split bulk polariton bands.

Numerical calculations were also performed on the tight-binding model to obtain the interface polariton dispersion (Fig. 2D and supplementary materials, section 1B). Topological interface states with Dirac type dispersion emerged spanning both the upper and lower bandgaps, with positive (negative) group velocities corresponding to the pseudospin-up (pseudospin-down) states, confirming their helical nature. FDTD simulations were performed on a WS_2-photonic crystal system with a topological domain wall (Fig. 2E and supplementary materials, section 2E). At the two Dirac points at 2.03 and 2.07 eV, the electromagnetic field is spatially confined to the topological interface, whereas in between, the field is found to spatially extend into the bulk lattice, corresponding to the central bulk polariton bands. The gap-spanning interface mode dispersion and the observation of the central bulk bands in the simulation further emphasize that the splitting in the topological interface polariton dispersion does not result from the gapping out of the interface state as in a topologically trivial system; instead, it is a natural phenomenon in a strongly coupled topological structure.

Experimentally, photonic crystals were patterned on suspended SiN_x membranes followed by transfer of monolayer WS_2 flakes (see the supplementary materials and methods) (Fig. 3A). The SiN_x photonic crystals were composed of six triangular holes arranged in a hexagonal lattice, in which the intercell and intracell interaction strengths were controlled by moving the holes toward or away from the unit cell center. The structure supports a TE electromagnetic mode with the pseudospin corresponding to the angular momentum of the out-of-plane ***H***-field, and hence the helicity of the in-plane ***E***-field at the center of each unit cell, which can be directly probed by a far-field circularly polarized light (*7*).

The energy-wavevector (E-k) dispersion of the topological polaritons was studied by angle-resolved reflectance measurements at 160 K. In this particular sample, the WS_2 A-exciton is located at 2.067 eV, in close resonance with ω_{ph} (detuning, δ_{ep} = –7 meV). Only at the topological interface is a set of unidirectional dispersion curves found between the upper and lower bulk polariton bands, with negative (positive) group velocities associated with the $\sigma^+(\sigma^-)$ polarizations, respectively, corresponding to the helical topological states (Fig. 3, B and C). Away from the interface, the unidirectional dispersion disappeared, leaving only the gapped bulk polariton bands (see the supplementary materials, section 3D). An anticrossing in the interface polariton dispersion curve was observed at the exciton energy, whereas the bulk central polariton bands were not observable because of low far-field coupling efficiency (see the supplementary materials, section 2D). All four interface bands with both helicities fit very well to the tight-binding model (Fig. 3D), resulting in a

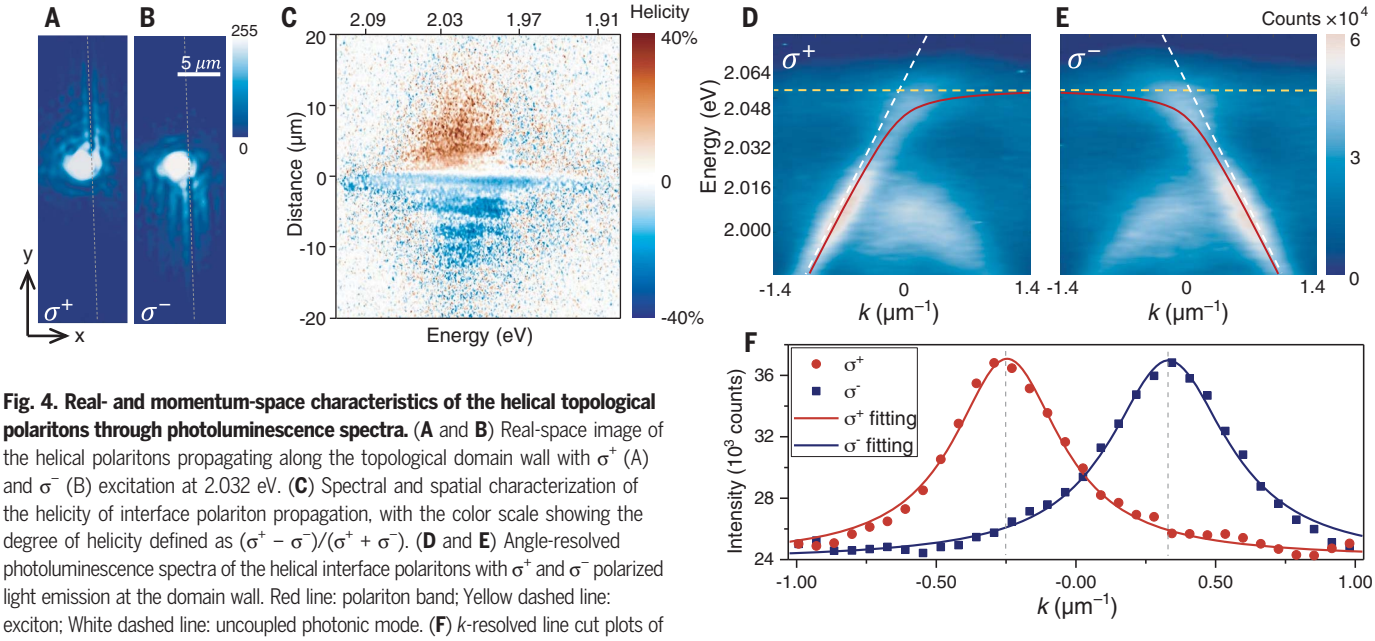

Fig. 4. Real- and momentum-space characteristics of the helical topological polaritons through photoluminescence spectra. (**A** and **B**) Real-space image of the helical polaritons propagating along the topological domain wall with σ^+ (A) and σ^- (B) excitation at 2.032 eV. (**C**) Spectral and spatial characterization of the helicity of interface polariton propagation, with the color scale showing the degree of helicity defined as $(\sigma^+ - \sigma^-)/(\sigma^+ + \sigma^-)$. (**D** and **E**) Angle-resolved photoluminescence spectra of the helical interface polaritons with σ^+ and σ^- polarized light emission at the domain wall. Red line: polariton band; Yellow dashed line: exciton; White dashed line: uncoupled photonic mode. (**F**) *k*-resolved line cut plots of (D) and (E) at $\hbar\omega$ = 2.032 eV and the corresponding single Lorentz peak fitting.

Rabi splitting Ω_{topo} = 38 ± 1 meV, suggesting that the system is in the strong coupling limit, given that γ_{ex} = 15 meV and γ_{ph} = 6.5 meV, satisfying the strong coupling criterion, $\Omega > \sqrt{2(\gamma_{ex}{}^2 + \gamma_{ph}{}^2)}$. It should be noted that in the bare photonic crystals, a small bandgap also exists in the dispersion of the interface states caused by the C_{6v} symmetry breaking at the interface (*26*). In our structure, this small gap (<3 meV) is much smaller than the polariton Rabi splitting, so it does not affect our analysis (see the supplementary materials, section 3H). In a different sample, interface-confined topological polariton formation was also confirmed with Ω_{topo} = 32 ± 1 meV (see the supplementary materials, section 3C) at 200 K. Therefore, these results demonstrate the realization of topological polaritons at relatively high temperatures because of the large exciton oscillator strength of monolayer WS_2 and the appropriately designed photonic structure. These topological polaritons have their in-plane momentum locked to the helicity of light, which are confined spatially at the interface and spectrally within the bulk bandgap, exhibiting striking differences from conventional exciton-photon polaritons and from the dispersion of the interface photonic modes. A Rabi splitting of Ω_{bulk} = 40 ± 1 meV was extracted from the same flake, which is comparable to Ω_{topo}, thus verifying our theoretical prediction that the Rabi splitting of the topological interface state is in accordance with that of the bulk (see the supplementary materials, section 3E).

The temperature-dependent polariton response was investigated by tuning the A-exciton energy from 77 to 180 K (Fig. 3, E and F). Both the upper and lower Dirac points red-shift with increasing temperature, which can be fitted to Eq. 4 at k_y = 0, resulting in a Rabi splitting Ω_{topo} = 38 ± 2 meV (Fig. 3F), consistent with the values extracted in Fig. 3D and those from the FDTD simulations (Fig. 2E). The mode shifting with temperature also demonstrates the ability to actively engineer the dispersion of the topological modes through the excitonic component. Precisely tuning the dispersion is critical in controlling the information transport speed, light-matter interaction strength, and nonlinear processes in devices, which is challenging in photonic topological systems. In polaritonic systems, the dispersion can be actively controlled spanning a broad parameter space by tuning the relative weights of excitons and photons. In the device demonstrated in Fig. 3, by changing the device temperature from 77 to 180 K, the group velocity can be tuned from 30 μm/ps to nearly 0, and effective polariton mass can be varied by two orders of magnitude within a 10 K range at a single operating wavelength and without breaking the topological protection of these modes (see the supplementary materials, section 3G).

Helical topological polariton transport was then studied in both the real and momentum space (Fig. 4) through real-space imaging and photoluminescence spectroscopy (see the supplementary materials and methods). The experiments were first performed at 200 K in a device with $\hbar\omega_{ex}$ = 2.055 eV and $\hbar\omega_{ph}$ = 2.060 eV with a circularly polarized laser ($\hbar\omega$ = 2.032 eV) incident at the topological domain wall. A real-space image was taken to directly visualize the waveguiding of the helical interface states, with the unidirectional, spin momentum–locked waveguiding along the interface readily observed (Fig. 4, A and B). By contrast, excitation in the bulk lattice region leads to no observable waveguiding at energies within the polaritonic bulk bandgap (see the supplementary materials, section 3J). Topological protection was also confirmed in a device with a domain wall with a 60° turn, and polaritons were successfully guided through the sharp turn without back scattering (see the supplementary materials, section 3I).

To investigate the spectral characteristics of the helical polariton propagation, the degree of circular polarization of the polariton emission was extracted as a function of energy and propagation distance along the interface (Fig. 4C; see the supplementary materials and methods). A large degree of helicity (33%) defined as $(\sigma^+ - \sigma^-)/(\sigma^+ + \sigma^-)$ was observed ~7.5 μm away from the excitation spot between ~1.98 and 2.05 eV, corresponding to the lower-branch helical interface polaritons. The degree of helicity is below unity because of the free exciton and trion emission excited directly by the pump laser, which leaks to the far field without coupling to the interface mode (see the detailed analysis in the supplementary materials, section 3K). The propagation length of helical polaritons at 2.023 eV is 8.0 ± 0.1 μm, which is mainly limited by the intrinsic far-field radiation loss of the photonic mode (see the supplementary materials, section 3K), purposely designed to enable the optical characterization of the system. Nonetheless, much longer propagation length can be achieved in devices with smaller photonic bandgap to reduce the radiation loss or by fabricating a valley Hall topological photonic crystal (*30*).

The polariton transport was further investigated in the momentum space through angle-resolved photoluminescence (Fig. 4, D and E)

measurements. At 200 K, photoluminescence from neutral A-excitons and negatively charged trions are observed at 2.055 and 2.015 eV, respectively. The strong coupling between the interface state and the neutral excitons can be identified by the anticrossing dispersion near the exciton energy and a redshift of the Dirac point from 2.060 eV in the uncoupled photonic mode, with the Rabi splitting Ω_{topo} of 32 ± 2 meV, confirming the strong coupling condition (see the supplementary materials, section 3F). The interface state and trions couple only weakly because of their smaller oscillator strength. To quantitatively investigate the degree of helicity of the topological interface exciton-polariton transport, the *k*-resolved line cuts at 2.032 eV corresponding to Fig. 4, D and E, are plotted in Fig. 4F. Both the interface modes corresponding to σ^+ and σ^- polarization fit to a single peak exclusively from the branch with positive and negative group velocities, respectively, thus demonstrating the helical nature of the topological polariton states.

Our approach of realizing strongly coupled topological polaritons opens the path to designing and eventually actively controlling the topological properties in a polaritonic system. Although the photonic topological devices are suitable for waveguides and transmission lines with low loss, by incorporating excitons, topological polaritons may find applications in low-threshold coherent light sources, nonlinear switchable and computational devices with precisely tailored dispersion and robust properties immune to defects. The design methodology presented here can be readily generalized to other topological structures such as 1D and 2D Su-Schrieffer–Heeger systems and higher-order topological states, to explore the rich topological physics in the strong coupling regime.

REFERENCES AND NOTES

1. M. Z. Hasan, C. L. Kane, *Rev. Mod. Phys.* **82**, 3045–3067 (2010).
2. F. D. M. Haldane, S. Raghu, *Phys. Rev. Lett.* **100**, 013904 (2008).
3. T. Ozawa *et al.*, *Rev. Mod. Phys.* **91**, 015006 (2019).
4. Z. Wang, Y. Chong, J. D. Joannopoulos, M. Soljačić, *Nature* **461**, 772–775 (2009).
5. M. Hafezi, S. Mittal, J. Fan, A. Migdall, J. M. Taylor, *Nat. Photonics* **7**, 1001–1005 (2013).
6. S. Barik *et al.*, *Science* **359**, 666–668 (2018).
7. N. Parappurath, F. Alpeggiani, L. Kuipers, E. Verhagen, *Sci. Adv.* **6**, eaaw4137 (2020).
8. T. Ma, A. B. Khanikaev, S. H. Mousavi, G. Shvets, *Phys. Rev. Lett.* **114**, 127401 (2015).
9. M. A. Bandres *et al.*, *Science* **359**, eaar4005 (2018).
10. Y. Zeng *et al.*, *Nature* **578**, 246–250 (2020).
11. T. Karzig, C.-E. Bardyn, N. H. Lindner, G. Refael, *Phys. Rev. X* **5**, 031001 (2015).
12. A. V. Nalitov, D. D. Solnyshkov, G. Malpuech, *Phys. Rev. Lett.* **114**, 116401 (2015).
13. C.-E. Bardyn, T. Karzig, G. Refael, T. C. H. Liew, *Phys. Rev. B* **91**, 161413 (2015).
14. Y. Zhang, Y. V. Kartashov, A. Ferrando, *Phys. Rev. A* **99**, 053836 (2019).
15. Y. V. Kartashov, D. V. Skryabin, *Phys. Rev. Lett.* **119**, 253904 (2017).
16. S. Klembt *et al.*, *Nature* **562**, 552–556 (2018).
17. A. Janot, B. Rosenow, G. Refael, *Phys. Rev. B* **93**, 161111 (2016).
18. C. Li *et al.*, *Phys. Rev. B* **97**, 081103 (2018).
19. G. Hu *et al.*, *Nature* **582**, 209–213 (2020).
20. M. Jung, Z. Fan, G. Shvets, *Phys. Rev. Lett.* **121**, 086807 (2018).
21. X. Liu *et al.*, *Nat. Photonics* **9**, 30–34 (2015).
22. L. Zhang, R. Gogna, W. Burg, E. Tutuc, H. Deng, *Nat. Commun.* **9**, 713 (2018).
23. S. Dufferwiel *et al.*, *Nat. Commun.* **6**, 8579 (2015).
24. Y.-J. Chen, J. D. Cain, T. K. Stanev, V. P. Dravid, N. P. Stern, *Nat. Photonics* **11**, 431–435 (2017).
25. W. Liu *et al.*, *Nano Lett.* **16**, 1262–1269 (2016).
26. L.-H. Wu, X. Hu, *Phys. Rev. Lett.* **114**, 223901 (2015).
27. S. Barik, H. Miyake, W. DeGottardi, E. Waks, M. Hafezi, *New J. Phys.* **18**, 113013 (2016).
28. W. Liu *et al.*, *Nano Lett.* **20**, 1329–1335 (2020).
29. Materials and methods are available as supplementary materials.
30. T. Ma, G. Shvets, *New J. Phys.* **18**, 025012 (2016).

ACKNOWLEDGMENTS

Funding: R.A. is supported by the US-ARO (grant no. W911NF-16-2-0194), ONR-MURI (grant no. N00014-17-1-2661), the National Science Foundation (NSF-QII-TAQS grant no. 1936276 and NSF 2-DARE grant no. EFMA-1542879), and by a seed grant from MRSEC/DMR-1720530. Device fabrication work was performed at the Singh Center for Nanotechnology at the University of Pennsylvania, which is supported by the NSF National Nanotechnology Coordinated Infrastructure Program under grant no. NNCI-1542153. A.P. is supported by the National Natural Science Foundation of China (grant nos. U19A2090 and 51525202).
Author contributions: R.A. supervised the project; W.L. and R.A. conceived the idea and designed the experiments; W.L. and Z.J. fabricated and characterized devices with help from Y.W. and G.M.; W.L., Y.W., and Z.J. performed optical measurements; W.L. developed the theoretical model and performed numerical simulations with help from Z.J., Y.W., and M.H.; B.Z. and A.P. grew the monolayer WS_2; V.J.S. provided input on waveguide characterization; and W.L. and R.A. analyzed the data and wrote the manuscript. All authors discussed the results and contributed to the final manuscript. **Competing interests:** The authors declare no competing interests. **Data and materials availability:** All data are available in the manuscript or the supplementary materials.

SUPPLEMENTARY MATERIALS

science.sciencemag.org/content/370/6516/600/suppl/DC1
Materials and Methods
Supplementary Text
Figs. S1 to S23
Tables S1 and S2
References (*31*–*36*)

28 April 2020; resubmitted 17 July 2020
Accepted 9 September 2020
Published online 8 October 2020
10.1126/science.abc4975

Generation of helical topological exciton-polaritons

Wenjing Liu, Zhurun Ji, Yuhui Wang, Gaurav Modi, Minsoo Hwang, Biyuan Zheng, Volker J. Sorger, Anlian Pan and Ritesh Agarwal

Science **370** (6516), 600-604.
DOI: 10.1126/science.abc4975originally published online October 8, 2020

Polaritons with a twist

The ability to design and fabricate optical systems with tunable topological features makes them especially attractive for developing analogs of topological condensed matter systems, which by themselves tend to be fixed or limited in their tunability. Liu *et al.* now show that the combination of a two-dimensional material with a photonic crystal can be used to develop an analogous quantum spin Hall system. The strong coupling between the monolayer tungsten disulfide excitons with a nontrivial hexagonal photonic crystal gives rise to helical topological polaritons observed at up to 200 kelvin. The topological polaritons can be actively tuned by temperature and may further be manipulated with electric or magnetic fields, thereby providing a flexible platform with which to explore exotic topological phenomena and new phases of quantum matter.

Science, this issue p. 600